Theoretical and Experimental Study of (Ba,Sr)TiO_3 Perovskite Solid Solutions and $BaTiO_3$/$SrTiO_3$ Heterostructures

Leonid L. Rusevich[1*], Guntars Zvejnieks[1], Eugene A. Kotomin[1], Marjeta Maček Kržmanc[2], Anton Meden[3], Špela Kunej[2], Ioana D. Vlaicu[4]

[1] Institute of Solid State Physics, University of Latvia, 8 Kengaraga str., Riga LV-1063, Latvia

[2] Advanced Materials Department, Jožef Stefan Institute, Jamova 39, 1000 Ljubljana, Slovenia

[3] Faculty of Chemistry and Chemical Technology, University of Ljubljana, Večna pot 113, Ljubljana 1001, Slovenia

[4] National Institute of Materials Physics, 405A Atomistilor Street, Magurele-Ilfov, 077125-Romania

Corresponding Author:

[*]E-mail: leorus@inbox.lv Phone: +371-67187480

Dr. Leonid L. Rusevich (Orcid ID: 0000-0002-4030-6157)

Prof. Dr. Eugene A. Kotomin (Orcid ID: 0000-0002-8122-6276)

Abstract

The results of experimental and theoretical *ab initio* study of structural and piezoelectric properties of (Ba,Sr)TiO_3 perovskite solid solutions are discussed and compared. Experimentally, plate-like (Ba,Sr)TiO_3 particles were synthesized by the topochemical conversion in the molten salt from $Bi_4Ti_3O_{12}$ template plates. All dimensions (side length ≈ 1 μm, thickness ≈ 200–400 nm) were well above the critical size necessary for observation of piezo- and ferroelectricity. The first-principles computations of the structural and electromechanical properties of solid solutions were performed with CRYSTAL14 computer code within the linear combination of atomic orbitals (LCAO) approximation, using three advanced hybrid functionals of the density-functional-theory (DFT). Different chemical compositions are considered for the ferroelectric and paraelectric phases. Calculated structural properties of solid solutions in tetragonal and cubic phases are in a very good agreement with experimental data. Experimentally obtained and calculated band gaps are compared for cubic $SrTiO_3$ and tetragonal $BaTiO_3$. $BaTiO_3$/$SrTiO_3$ heterostructures were considered theoretically for different chemical compositions. The calculated piezoelectric properties of solid solutions and heterostructures in ferroelectric phase are compared. It is predicted that both solid solutions and heterostructures improve the piezoelectric properties of the bulk $BaTiO_3$, but solid solutions are more preferable for equal Sr concentrations.

Introduction

Nowadays development of devices for energy storage applications, for the harvesting and mutual transformations of mechanical and electrical energies is of great interest. In this respect, the utilizing of piezoelectricity is the efficient way,[1] and, therefore, ferroelectric perovskites are important materials for many technological applications. For a long time lead-zirconate-titanate (PZT) is the most widely used piezoelectric material for electromechanical applications.[2,3] However, due to Pb toxicity, it is challenging problem to develop lead-free ceramics with good piezoelectric properties. Recently several lead-free piezoelectrics were investigated.[4,5] $BaTiO_3$-based (BTO) piezoelectric materials are considered as potential substitution for PZT.[6,7] Most studies on biocompatible piezoelectrics have also focused on BTO-based materials.[8] Although pure BTO exhibits fairly low piezoelectric properties (and temperature stability of these properties) in comparison with PZT, further design could allow material improvement. This design may include domains, defects, phase boundary engineering and texturing (ref 6 and references therein). Functional properties of BTO-based materials are sensitive to chemical modifications. In particular, significant improvement of piezoelectric and dielectric properties was found in binary and ternary Sr-, Ca- and Zr-modified BTO-based solid solutions.[6,9,10] To optimize the functional properties of BTO perovskite, the $BaTiO_3/SrTiO_3$ (BTO/STO) ferroelectric plates (heterostructures) could be also used.[6,11]

At high temperatures, BTO has a cubic structure with Ti ions octahedrally coordinated with 6 nearest oxygen ions. It is structure with centrosymmetric *Pm-3m* space group (SG 221), and therefore it is both paraelectric and non-piezoelectric. As the temperature decreases, Ti ions are displaced from the cube center, which leads (at ambient pressure — at 393 K) to a paraelectric-ferroelectric and structural phase transition with spontaneous polarization directed parallel to the tetragonal edge of the pseudocubic unit cell. At this transition crystal symmetry reduces from

cubic (SG 221) to tetragonal (*P4mm*, SG 99). At further cooling BTO undergoes two consecutive inter-ferroelectric structural transitions: to orthorhombic phase (*Amm2*, SG 38) at 278 K and to rhombohedral phase (*R3m*, SG 160) below 183 K. Direction of spontaneous polarization at these transitions re-orients along a face diagonal (orthorhombic) and body diagonal (rhombohedral) of unit cell. All three phase transitions in BTO are of first-order.

Important aspect in improvement of functional properties of materials is the possibility to perform computations of structural, electronic and electromechanical properties of perovskites based on *ab initio* (first-principles) approach. Several calculations of functional properties of BTO crystals have been reported.[12-14] Recently we performed the first theoretical study of the electromechanical/piezoelectric properties of the tetragonal $Ba_{(1-x)}Sr_xTiO_3$ (BSTO) ferroelectric solid solution by means of first-principles calculations.[15] Our calculations for chemical compositions x=0.125 and x=0.25 show that the Sr-doping of BTO enhances its piezoelectric properties.

As experimentally known,[16,17] at $x\approx0.3$ (at room temperature) BSTO reveals phase transition from tetragonal to cubic phase (i.e. ferroelectric-paraelectric transition), which means that for higher Sr concentrations this solid solution has a cubic symmetry without piezoelectric properties. At the same time, BTO/STO heterostructures still remain ferroelectric even at high Sr concentration (ref 18 and references therein). In this paper preparation and structural properties of complex BSTO perovskites are discussed. We analyze the structural parameters of tetragonal (the most important for applications) and cubic BSTO room temperature phases. Additionally, we theoretically considered BTO/STO heterostructures with the same chemical compositions as solid solutions in ferroelectric phase (x<0.3).

Experiment

Plate-like BSTO particles were synthesized using two-stage reaction process in the molten salt. At the first step, $Bi_4Ti_3O_{12}$ plates were synthesized from Bi_2O_3 and TiO_2 nanopowders in the molten salt (NaCl:KCl=1:1) at 800°C for 2 hours. At the second stage, these $Bi_4Ti_3O_{12}$ plate-like particles were used as the template for the preparation of BSTO plates via topochemical transformation in the molten salt with the following ratio of the reagents: KCl:NaCl:$Bi_4Ti_3O_{12}$:($BaCO_3$+$SrCO_3$)=39:39:1:10. The reactions were performed at the following heat treatment conditions: heating 10°C/min to 600°C and 0.5°C/min to 900°C, isothermal annealing for 2 hours at this temperature and cooling 1°C/min to room temperature. Pure BSTO plates were obtained after the removal of salt by washing with water and elimination of side products by sedimentation and washing with HNO_3 (2 M). The final BSTO composition was tailored, based on the experimentally determined relationship between Ba/Sr ratio in the initial reaction mixture and the Ba/Sr in the formed perovskite plates. Synthesis procedure is described in details in ref 19 and ref 20.

The morphology and actual composition of BSTO plate-like particles were investigated using the field-emission scanning electron microscope (FE-SEM, JSM-7600 F, JEOL) equipped with the Oxford Instruments Inca energy-dispersive X-ray spectrometer (EDS). The unit cell parameters were determined from X-ray powder diffraction patterns, collected on a PANalytical X'pert PRO MPD X-ray powder diffractometer. Pure Cu–$K_{\alpha 1}$ radiation with λ=1.5406 Å and high resolution were ensured by Johansson type primary monochromator. Rietveld refinement was used to calculate the unit-cell parameters. Tetragonal structure (SG 99, collection code 237105 from the ICSD database) was loaded into the program and only the background coefficients, profile parameters and unit cell parameters were refined. The atomic coordinates

were fixed, as well as the population parameters, which were calculated from the chemical composition, found by EDS. Profile R_{wp} showed good agreement on all cases (between 10% and 15%) and in the cases where the samples were actually cubic, this was clearly seen from the value of the, *c/a* ratio, which was very close to 1 in such cases.

The optical band gaps for direct and indirect transitions in tetragonal BTO and cubic STO plate-like particles were determined from the diffuse reflectance spectra using the Kubelka-Munk method. Spectroscopic measurements were performed using a UV-Vis-NIR spectrophotometer (Shimadzu UV-3600) equipped with an integrating sphere (ISR-3100, 60 mm, Shimadzu); $BaSO_4$ standard was used as the reference.

Computational Details

Computational details of our calculations are described in details in our previous paper.[15] Here we will outline only basic moments and specific details. The quantum chemical computer code CRYSTAL14 suitable for *ab initio* materials modelling[21] was used within the linear combination of atomic orbitals (LCAO) approximation of the density functional theory (DFT). The small core effective pseudopotentials are used for Ba, Ti and Sr atoms,[22] while all-electron basis set is used for O atoms.[23] Calculations are performed with three commonly used hybrid exchange-correlation functionals.[24] One is PBE0,[25] where PBE exchange functional is combined with 25% of Hartree-Fock (HF) exchange and the PBE correlation functional. The second — B1WC functional,[26] which combines Wu-Cohen WCGGA exchange functional with 16% of HF exchange and the Perdew-Wang PWGGA correlation functional. Lastly, the third, B3LYP functional, is a three parameter functional, combining BECKE exchange functional with 20% of HF exchange and LYP (Lee-Yang-Parr) correlation functional (NONLOCAL parameters are 0.9 and 0.81).[24]

A 2×2×2 supercell of the tetragonal (SG 99) or cubic (SG 221), depending on Sr concentration, BTO unit cell is used as computational model for the BSTO solid solution. This supercell consists of 40 atoms (eight primitive unit cells). In the supercell calculations, we modelled artificially ordered $Ba_{(1-x)}Sr_xTiO_3$ solid solutions using a series of different compositions (i.e. Sr/Ba ratio), where Ba atoms are progressively replaced by Sr atoms. With tetragonal supercell, we considered three different Sr concentrations: pure BTO (without substitution, x=0.0); one Ba atom is replaced with Sr atom (x=0.125); two Ba atoms are replaced with Sr atoms (x=0.25). The computations for six more Sr concentrations (x=0.375, 0.5, … 1, where x=1 is the case of pure STO) were performed with cubic supercell according to that fact, that for compositions with $x\geq0.3$ BSTO solid solution has a cubic symmetry. In order to preserve symmetry, for the x=0.125 composition we replaced Ba atom at the coordinate origin *(0,0,0)*, whereas for the x=0.25 — the first atom at the origin and second with coordinates *(0.5, 0.5, 0.5)*. In general, we have 7 different possibilities for the substitution of second atom. But, as it was pointed in ref 15, the effect of configurational disorder (different configurations of atoms) on BSTO is small (less than 4% for results of calculations by PBE0 functional of elastic and piezoelectric properties and significantly less for structural properties), therefore we do not take into account this effect in current work and consider for x=0.25 only one, mentioned above, configuration of atoms (see ref 15 for details). For the same reason in cubic structures (x>0.3) we only retain cubic symmetry in replacing of Ba atoms with Sr atoms and restrict ourselves to a single configuration for each chemical composition.

Computational model for the BTO/STO heterostructure is the 1×1×n supercell of the tetragonal (SG 99) BTO unit cell. Thus, we consider the superlattice $(BTO)_k/(STO)_l$, where k and l refer to the thickness (in unit cells) of BTO and STO layers, respectively, and $k+l=n$ (i.e., we replace in the supercell l of consecutive Ba atoms with Sr atoms). This superlattice is repeated

along z axis m times, i.e., it is $[(BTO)_k/(STO)_l]_m$ structure; in our computations $m=\infty$. To calculate heterostructures with the same chemical compositions, as in solid solutions (x=0.0, 0.125 and 0.25), we used 8-layer (n=8) structures — $(BTO)_8$, $(BTO)_7/(STO)_1$ and $(BTO)_6/(STO)_2$, respectively.

Computation of direct and converse piezoelectricity (using the Berry phase approach) is implemented in CRYSTAL14 as a fully automated procedure.[24]

Results and Discussion

The composition of experimentally grown BSTO plate-like particles was found to be different from that, expected from the $BaCO_3/SrCO_3$ ratio in the initial reaction mixture. Nevertheless, this topochemical conversion reaction is reasonable because all side products were possible to be eliminated enabling preparation of pure perovskite defined shape particles with negligible Bi remains (< 0.9 at. %). Additionally, an arbitrary solid solution with $0 \le x \le 0.82$ ($0 \le x' \le 0.3$ in the initial reaction mixture) could be prepared based on the experimentally determined relationship $x \approx 2.7x'$ (see ref 20). Detailed analysis of the compositional dependence of the unit cell parameters, obtained by the Rietveld refinement of the room temperature X-ray diffraction patterns, revealed that unit cell volume decreases nearly linearly with an increase of Sr content. Similarly, the c/a ratio (characterizing tetragonal distortion) linearly decreases from 1.0092 (x=0) to 1.0037 (x=0.23) and then stabilized at c/a=1 (cubic structure) for $0.23 < x \le 1$ (Table 1).

Table 1. Experimental Dependence of Unit Cell Structural Parameters (Lattice Constants *a*, *c* and Volume *V*) of $Ba_{(1-x)}Sr_xTiO_3$ Plates, Obtained by the Topochemical Conversion, on Composition *x*.

x	*a*, Å	*c*, Å	*c/a*	*V*, Å^3
0	3.9983(1)	4.0352(1)	1.0092	64.507(3)
0.054	3.9937(1)	4.0271(1)	1.0084	64.230(3)
0.11	3.9872(1)	4.0144(1)	1.0068	63.821(3)
0.175	3.9817(1)	4.0027(1)	1.0053	63.459(3)
0.23	3.9756(1)	3.9904(1)	1.0037	63.071(3)
0.38	3.9656(1)	3.9630(1)	0.9993	62.324(3)
0.53	3.9511(1)	3.9504(1)	0.9998	61.671(3)
0.82	3.9218(1)	3.9215(1)	0.9999	60.315(3)
0.95	3.9092(1)	3.9096(1)	1.0001	59.744(3)
1	3.9065(1)	3.9053(1)	0.9997	59.597(3)

Numbers in parentheses are standard deviations at the last given digit.

In contrast to $Ba_{(1-x)}Sr_xTiO_3$ with $0 \le x \le 0.11$, which exhibits a clear tetragonal splitting and significant ferroelectric and piezoelectric characteristics as determined by differential scanning calorimetry (DSC) and piezoresponce force microscope (PFM) investigations, the composition with x=0.175 showed weak ferroelectric and piezoelectric response observed only by PFM but not by DSC. Although the composition with x=0.23 exhibits some small tetragonality (c/a=1.0037), no ferroelectric and piezoelectric effects was detected by PFM for this composition at room temperature.[20]

Before theoretical investigating of BSTO solid solutions, we calculated the lattice constants and band gaps for pure bulk BTO and STO crystals. The obtained results for the cubic (SG 221) phases of BTO and STO are given in Table 2, where they are compared also with experimental data, obtained in this study and taken from the literature.

Table 2. Parameters of Cubic Phases of BTO and STO — Lattice Constant *a* and Band Gap E_g — Calculated Using Three Hybrid Functionals.

	PBE0	B1WC	B3LYP	Expt
BTO, SG 221				
a, Å	3.993	3.975	4.037	3.996[27]
E_g[a], eV	3.97 (4.00)	3.20 (3.24)	3.48 (3.55)	3.2[28]
STO, SG 221				
a, Å	3.901	3.884	3.937	3.906;[b] 3.905[29]
E_g[a], eV	4.16 (4.47)	3.36 (3.68)	3.67 (3.98)	3.19 (3.33);[b] 3.25 (3.75)[30]

Expt — experimental data. The experimental band gap[28] at the temperature ≈ 130°C.
[a]Indirect (direct) band gap; [b]this study.

As one can see from Table 2, for the both crystals the PBE0 functional gives the best agreement with experimental value for lattice constant *a*, while B3LYP functional shows the worst agreement. For both BTO and STO in their cubic phases, calculations yield indirect band gaps. The band gaps, calculated by means of the B1WC functional, are very close to experimental data for both crystals.

The results of our calculations of structural properties and band gap for BTO crystal in tetragonal phase as well as direct (e_{33}) and converse (d_{33}) piezoelectric constants along with experimental data are given in Table 3.

Table 3. The BTO Structural Properties, Band Gap and Piezoelectric Constants (Tetragonal Phase, SG 99).

	PBE0	B1WC	B3LYP	Expt
lattice constants				
a=b, Å	3.971	3.962	3.991	3.998;[a] 3.992[27]
c, Å	4.131	4.050	4.292	4.035;[a] 4.036[27]
c/a	1.040	1.022	1.075	1.009;[a] 1.011[27]
band gap				
E_g[b], eV	4.08 (4.52)	3.26 (3.60)	3.62 (4.18)	2.98 (3.23);[a] 3.38 (3.27)[28]
piezoelectric constants				
e_{33}, C/m^2	3.3	4.2	2.6	6.7[31]
d_{33}, pm/V	37.0	32.7	57.3	85.6;[32] 90[33]

[a]This study. [b]Indirect (direct) band gap for calculated and experimental values, obtained in this study; experimental data[28] at room temperature for light polarized parallel (perpendicular) to the ferroelectric *c* axis.

Table 3 reveals that B3LYP functional gives better agreement with experimental data for *a=b* lattice constant, but the worst for *c* constant and the tetragonal ratio *c/a*. At the same time, B1WC functional gives the best agreement for *c* constant and for *c/a* ratio (discrepancy with experimental value is ~1%). Concerning the band gap, the B1WC functional gives again the result, which is closer to experimental data, and, thus, we conclude that B1WC functional reproduces correctly experimental band gap (though, even it gives slightly overestimated values for band gaps in comparison with experimental data).

The origin of the piezoelectricity in BTO is related mainly to the atomic relaxations with a small electronic "clamped-ion" contribution.[15] For each piezoelectric tensor — direct and converse — we show in Table 3 only one constant, the most often defined in experiments. Table 3 demonstrates a considerable discrepancy between theory and experiments on piezoelectric constants. Note, however, that we performed calculations for a single domain crystal, while in real materials domain sizes and movement of domain walls can be by major

factors, determining piezoelectric properties of samples.[6] Therefore, the analysis should be concentrated on the general trend in the behavior of the piezoelectric constants.

Based on our theoretical calculations by three functionals for three Sr concentrations (x=0.0, 0.125, 0.25) and experimental data (Table 1), for tetragonal phase of BSTO dependences c/a vs. x and V (unit cell volume) vs. x were plotted in Figure 1 and Figure 2, respectively.

As one can see in Figure 1, close to the linear dependences of c/a vs. x (Sr concentration) take place for both theoretical and experimental results (R-squared displacement for experimental data is 0.9937, for PBE0, B1WC and B3LYP functionals — 0.9973, 1.0 and 0.9796, respectively); theoretical data are overestimated for all functionals; the best agreement with experiment (for c/a and slope) is demonstrated by the B1WC functional.

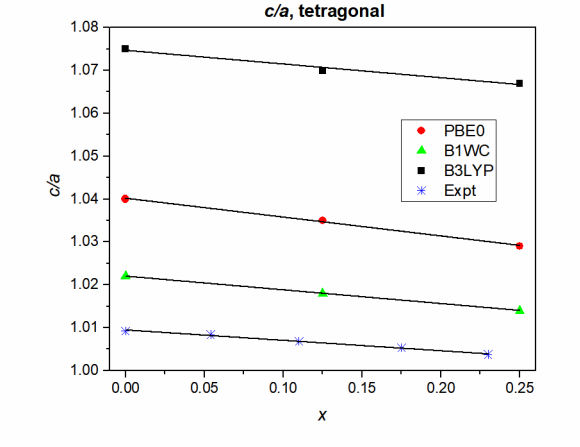

Figure 1. Theoretical and experimental dependences of tetragonal ratio c/a vs. chemical compositions x (Sr doping) for tetragonal phase of BSTO. The lines — linear fitting.

Similar analysis for the volume of unit cell (Figure 2) reveals again close to the linear dependences ($<R^2>$ for experimental data is 0.9975, 1 — for PBE0 and B1WC functional, 0.9997

— for B3LYP functional) and demonstrates very good agreement between experimental and theoretical data; PBE0 functional shows the best agreement with experiment.

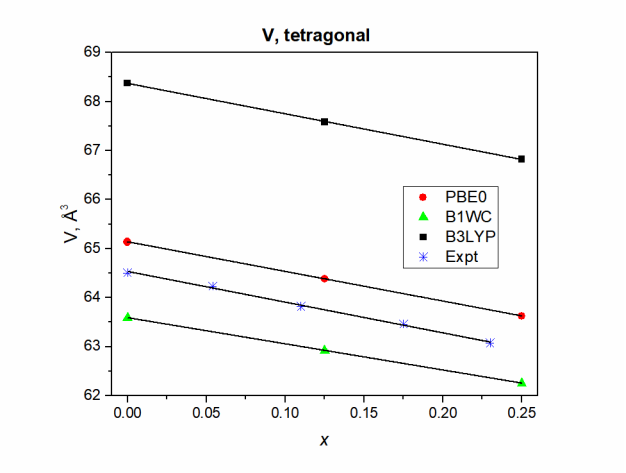

Figure 2. Theoretical and experimental dependences of unit cell volume *V* vs. chemical compositions *x* for tetragonal phase of BSTO. The lines — linear fitting.

Let us consider now the cubic phase of BSTO solid solution (observed experimentally at high Sr concentrations, $x>0.3$). Using theoretical calculations with three functionals for cubic phase and the experimental data (Table 1), dependences *a* (lattice constant) vs. *x* were plotted in Figure 3.

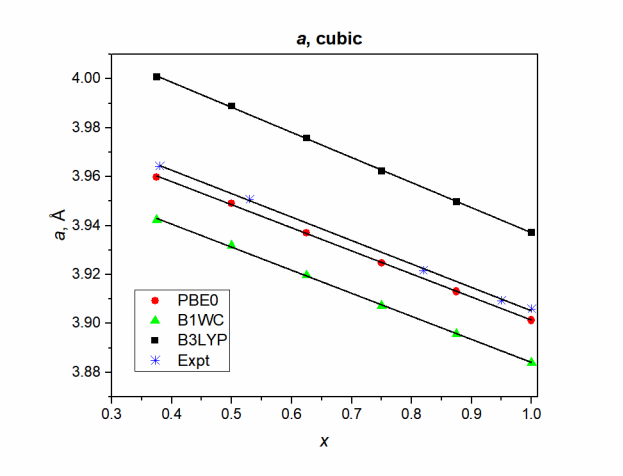

Figure 3. Theoretical and experimental dependences of lattice constant *a* vs. chemical compositions *x* for cubic phase of BSTO. The lines — linear fitting.

One can see the linear dependence *a* vs. *x* for both theoretical and experimental data; these dependences are fulfilled with high accuracy: $<R^2>$ for experimental data is 0.9993, for theoretical — within the range of 0.9995–0.9997. Note the excellent agreement between calculated and experimental data; in particular, PBE0 functional shows remarkable coincidence with the experiment (difference between experimental and theoretical values *a* is ~0.1%). Based on theoretical computations of BSTO cubic structure, we found very accurate implementation of the Vegard's law for the lattice constant *a* of the cubic phase of BSTO, calculated by all three functionals.

Lastly, let us discuss piezoelectric constants of BSTO solid solutions and BTO/STO heterostructures calculated for different compositions. We compare their piezoelectric properties for identical dopant concentrations $0 \leq x \leq 0.25$ when solid solutions show piezoelectric properties (more detailed general study of the heterostructures will be published separately). The results, calculated using the PBE0 functional, for heterostructures and solid solutions with the same chemical compositions (Sr/Ba ratio ≤ 0.25) are given in Table 4. $(BTO)_8$ for heterostructure and

x=0 for solid solution are different ways of calculation the bulk BTO and, thus, the results have to be identical, what Table 4 reveals with high accuracy.

Table 4. Piezoelectric Constants for BTO/STO Heterostructures and BSTO Solid Solutions, Calculated by PBE0 Functional.

BTO/STO heterostructures					
	$(BTO)_8$	$(BTO)_7/(STO)_1$	%	$(BTO)_6/(STO)_2$	%
e_{33}, C/m^2	3.295	3.564	8.2%	3.841	16.6%
d_{33}, pm/V	36.992	37.838	2.3%	38.518	4.1%
BSTO solid solutions					
	x=0	*x*=0.125	%	*x*=0.25	%
e_{33}, C/m^2	3.294	3.720	12.9%	4.270	29.6%
d_{33}, pm/V	36.987	39.594	7.0%	42.404	14.6%

% — gain of piezoelectric constants with regard to pure BTO systems ($(BTO)_8$ or *x*=0).

One can see from Table 4 that piezoelectric constants demonstrate growth upon substitution of Ba with Sr atoms both for solid solution and for heterostructure, but solid solutions are more preferable at considered Sr concentrations. Indeed, for solid solution at *x*=0.25 we see enhancement (in comparison with *x*=0) of e_{33} and d_{33} piezoelectric constants by 30% and 15%, respectively, and only by 17% (e_{33}) and 4% (d_{33}) for heterostructure. The same trend remains in calculations with B1WC functional.

Conclusions

A-site-substituted ($ATiO_3$) complex perovskite BSTO plate-like particles were synthesized by a topochemical conversion reaction in a molten salt. The relationship between the actual and proposed Sr concentrations was determined. The experimental study was focused on the examination of the structural properties of the BSTO particles depending on chemical

composition *x*. Moreover, optical band gaps for cubic phase of STO and tetragonal phase of BTO were measured. The results of the experimental and theoretical studies of the structural changes in BSTO solid solutions with different Sr concentrations (for tetragonal and cubic phases) agree very well each with other for the lattice constants, volumes, and tetragonality parameter *c/a*. It demonstrates that the synthesized plate-like particles are large enough to be considered as the nearly bulk material. We have shown that both the PBE0 and B1WC hybrid functionals are quite suitable for description of structural parameters of BSTO for different chemical compositions and B1WC functional gives the best results for the band gaps.

It is theoretically predicted that both solid solutions and heterostructures improve the piezoelectric properties of bulk BTO, but solid solutions in their ferroelectric phase are more efficient than heterostructures for the same Sr concentrations.

Acknowledgements

This study was supported by the ERA-NET HarvEnPiez project. The authors would like to thank their national funding agencies (Latvian State Education Development Agency, Slovenian Ministry of Higher Education, Science and Technology, Romanian National Authority for Scientific Research and Innovation, CCCDI-UEFISCDI, project number 49/2016 within PNCDI III – M-ERA NET Program).

References

1. Bowen, C. R.; Kim, H. A.; Weaver, P. M.; Dunn, S. Piezoelectric and Ferroelectric Materials and Structures for Energy Harvesting Applications. *Energy Environ. Sci.* **2014**, *7*, 25–44.
2. Jaffe, B.; Cook, W. R.; Jaffe, H. *Piezoelectric Ceramics*; Academic Press: London, 1971.
3. Damjanovic, D. Ferroelectric, Dielectric and Piezoelectric Properties of Ferroelectric Thin Films and Ceramics. *Rep. Prog. Phys.* **1998**, *61*, 1267–1324.
4. Rödel, J.; Jo, W.; Seifert, K. T. P.; Anton, E-M.; Granzow, T.; Damjanovic, D. Perspective on the Development of Lead-Free Piezoceramics. *J. Am. Ceram. Soc.* **2009**, *92*, 1153–1177.
5. Mahajan, A.; Zhang, H.; Wu, J.; Ramana, E. V.; Reece, M. J.; Yan, H. Effect of Phase Transitions on Thermal Depoling in Lead-Free $0.94(Bi_{0.5}Na_{0.5}TiO_3)$-$0.06(BaTiO_3)$ Based Piezoelectrics. *J. Phys. Chem. C* **2017**, *121*, 5709–5718.
6. Acosta, M.; Novak, N.; Rojas, V.; Patel, S.; Vaish, R.; Koruza, J.; Rossetti, G. A., Jr.; Rödel, J. $BaTiO_3$-Based Piezoelectrics: Fundamentals, Current Status, and Perspectives. *Appl. Phys. Rev.* **2017**, *4*, 041305.
7. Gao, J.; Xue, D.; Liu, W.; Zhou, C.; Ren, X. Recent Progress on $BaTiO_3$-Based Piezoelectric Ceramics for Actuator Applications. *Actuators* **2017**, *6*, 24.
8. Baxter, F. R.; Bowen, C. R.; Turner, I. G.; Dent, A. C. E. Electrically Active Bioceramics: A Review of Interfacial Responses. *Ann. Biomed. Eng.* **2010**, *38*, 2079–2092.
9. Fu, D.; Itoh, M.; Koshihara S. Crystal Growth and Piezoelectricity of $BaTiO_3$-$CaTiO_3$ Solid Solution. *Appl. Phys. Lett.* **2008**, *93*, 012904.
10. Dong, L.; Stone, D. S.; Lakes, S. Enhanced Dielectric and Piezoelectric Properties of $x$$BaZrO_3$-$(1-x)BaTiO_3$ Ceramics. *J. Appl. Phys.* **2012**, *111*, 084107.

11. Schlom, D. G.; Chen, L-Q.; Eom, C-B.; Rabe, K. M.; Streiffer, S. K.; Triscone, J-M. Strain Tuning of Ferroelectric Thin Films. *Annu. Rev. Mater. Res.* **2007**, *37*, 589–626.
12. Khalal, A.; Khatib, D.; Jannot, B. Elastic and Piezoelectric Properties of $BaTiO_3$ at Room Temperature. *Physica B* **1999**, *271*, 343–347.
13. Meng, X.; Wen, X.; Qin, G. DFT Study on Elastic and Piezoelectric Properties of Tetragonal $BaTiO_3$. *Comput. Mater. Sci.* **2010**, *49*, S372–S377.
14. Mahmoud, A.; Erba, A.; El-Kelany, K. E.; Rerat, M.; Orlando, R. Low-Temperature Phase of $BaTiO_3$: Piezoelectric, Dielectric, Elastic, and Photoelastic Properties from *Ab Initio* Simulations. *Phys. Rev. B* **2014**, *89*, 045103.
15. Rusevich, L. L.; Zvejnieks, G.; Erba, A.; Dovesi, R.; Kotomin, E. A. Electromechanical Properties of $Ba_{(1-x)}Sr_xTiO_3$ Perovskite Solid Solutions from First-Principles Calculations. *J. Phys. Chem. A* **2017**, *121*, 9409–9414.
16. Lemanov, V. V.; Smirnova, E. P.; Syrnikov, P. P.; Tarakanov, E. A. Phase Transitions and Glasslike Behavior in $Sr_{1-x}Ba_xTiO_3$. *Phys. Rev. B* **1996**, *54*, 3151–3157.
17. Kim, S. W.; Choi, H. I.; Lee, M. H.; Park, J. S.; Kim, D. J.; Do, D.; Kim, M. H.; Song, T. K.; Kim, W. J. Electrical Properties and Phase of $BaTiO_3$-$SrTiO_3$ Solid Solution. *Ceram. Int.* **2013**, *39*, S487−S490.
18. Schlom, D. G.; Chen, L-Q.; Fennie, C. J.; Gopalan, V.; Muller, D. A.; Pan, X.; Ramesh, R.; Uecker, R. Elastic Strain Engineering of Ferroic Oxides. *MRS Bull.* **2014**, *39*, 118–130.
19. Kržmanc, M. M.; Jančar, B.; Uršič, H.; Tramšek, M.; Suvorov, D. Tailoring the Shape, Size, Crystal Structure, and Preferential Growth Orientation of $BaTiO_3$ Plates Synthesized Through a Topochemical Conversion Process. *Cryst. Growth Des.* **2017**, *17*, 3210–3220.

20. Kržmanc, M. M.; Uršič, H.; Meden, A.; Korošec, R. C.; Suvorov, D. $Ba_{1-x}Sr_xTiO_3$ plates: Synthesis through Topochemical Conversion, Piezoelectric and Ferroelectric Characteristics. *Ceram. Int.* **2018**, *44*, 21406–21414.
21. Dovesi, R.; Orlando, R.; Erba, A.; Zicovich-Wilson, C. M.; Civalleri, B.; Casassa, S.; Maschio, L.; Ferrabone, M.; De La Pierre, M.; D'Arco, P.; et al. CRYSTAL14: A Program for the *Ab Initio* Investigation of Crystalline Solids. *Int. J. Quantum Chem.* **2014**, *114*, 1287−1317.
22. Piskunov, S.; Heifets, E.; Eglitis, R. I.; Borstel, G. Bulk Properties and Electronic Structure of $SrTiO_3$, $BaTiO_3$, $PbTiO_3$ Perovskites: An *Ab Initio* HF/DFT Study. *Comput. Mater. Sci.* **2004**, *29*, 165–178.
23. Bredow, T.; Jug, K.; Evarestov, R. A. Electronic and Magnetic Structure of $ScMnO_3$. *Phys. Stat. Sol. (b)* **2006**, *243*, R10−R12.
24. Dovesi, R.; Saunders, V. R.; Roetti, C.; Orlando, R.; Zicovich-Wilson, C. M.; Pascale, F.; Civalleri, B.; Doll, K.; Harrison, N. M.; Bush, I. J.; et al. *CRYSTAL14 User's Manual*; University of Torino: Torino, Italy, 2014.
25. Adamo, C.; Barone, V. Toward Reliable Density Functional Methods without Adjustable Parameters: The PBE0 Model. *J. Chem. Phys.* **1999**, *110*, 6158−6170.
26. Bilc, D. I.; Orlando, R.; Shaltaf, R.; Rignanese, G. M.; Iniguez, J.; Ghosez, Ph. Hybrid Exchange-Correlation Functional for Accurate Prediction of the Electronic and Structural Properties of Ferroelectric Oxides. *Phys. Rev. B* **2008**, *77*, 165107.
27. In *Ternary Compounds, Organic Semiconductors*; Madelung, O., Rössler, U., Schulz, M., Eds.; Landolt-Börnstein — Group III Condensed Matter; Springer: Berlin, 2000; Vol. *41E*.
28. Wemple, S. H. Polarization Fluctuations and the Optical-Absorption Edge in $BaTiO_3$. *Phys. Rev. B* **1970**, *2*, 2679–2689.

29. Cao, L.; Sozontov, E.; Zegenhagen, J. Cubic to Tetragonal Phase Transition of $SrTiO_3$ under Epitaxial Stress: An X-Ray Backscattering Study. *Phys. Stat. Sol. (a)* **2000**, *181*, 387−404.
30. van Benthem, K.; Elsässer, C.; French, R. H. Bulk Electronic Structure of $SrTiO_3$: Experiment and Theory. *J. Appl. Phys.* **2001**, *90*, 6156−6164.
31. Zgonik, M.; Bernasconi, P.; Duelli, M.; Schlesser, R.; Günter, P.; Garrett, M. H.; Rytz, D.; Zhu, Y.; Wu, X. Dielectric, Elastic, Piezoelectric, Electro-Optic, and Elasto-Optic Tensors of $BaTiO_3$ Crystals. *Phys. Rev. B* **1994**, *50*, 5941−5949.
32. Berlincourt, D.; Jaffe, H. Elastic and Piezoelectric Coefficients of Single-Crystal Barium Titanate. *Phys. Rev.* **1958**, *111*, 143–148.
33. Davis, M.; Budimir, M.; Damjanovic, D.; Setter, N. Rotator and Extender Ferroelectrics: Importance of the Shear Coefficient to the Piezoelectric Properties of Domain-Engineered Crystals and Ceramics. *J. Appl. Phys.* **2007**, *101*, 054112.

TOC Graphic

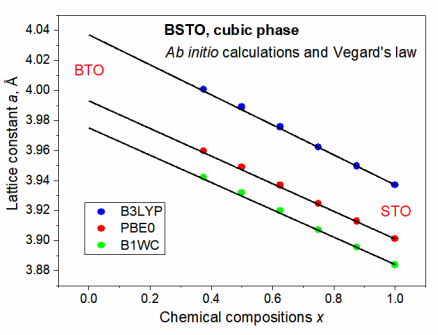

Institute of Solid State Physics, University of Latvia as the Center of Excellence has received funding from the European Union's Horizon 2020 Framework Programme H2020-WIDESPREAD-01-2016-2017-TeamingPhase2 under grant agreement No. 739508, project CAMART²